

## Structure of the Cytoplasmic Domain of p23 in Solution: Implications for the Formation of COPI Vesicles

Marcus Weidler,\*<sup>1</sup> Constanze Reinhard,† Gabi Friedrich,\* Felix T. Wieland,† and Paul Rösch\*

\*Lehrstuhl für Biopolymere, Universität Bayreuth, Germany; and †Biochemie-Zentrum Heidelberg, Ruprecht-Karls-Universität Heidelberg, Heidelberg, Germany

Received January 3, 2000

**Coatmer, the coat protein complex of coat protein (COPI) vesicles, is involved in the budding of these vesicles. Its interaction with the cytoplasmic domains of some p24-family members, type I transmembrane proteins of the Golgi, has been shown to induce a conformational change of coatmer that initiates polymerization of the complex. From stoichiometrical data it is likely that interaction of coatmer with the small tail domains involves an oligomeric form of the p24 proteins. Here we present the structure of peptide analogs of the cytoplasmic domain of p23, a member of the p24 family, as determined by two-dimensional nuclear magnetic resonance spectroscopy in the presence of 2,2,2-trifluoroethanol. An improved strategy for structure calculation revealed that the tail domain peptides form  $\alpha$ -helices and adopt a tetrameric state. Based on these results we propose an initial model for the binding of coatmer by p23 and the induced conformational change of coatmer that results in its polymerization, curvature of the Golgi membrane to form a bud, and finally a COPI-coated vesicle.** © 2000

Academic Press

**Key Words:** NMR; coatmer; p23; formation of vesicles.

Two types of coat protein complexes have been described for the secretory pathway, COPI and COPII (coat protein), differing in their protein subunits. COPI-coated vesicles mediate protein transport in the early secretory pathway [1–3]. The COPI coat consists of a small G protein, ADP-ribosylation factor 1 (ARF1) [4, 5] and coatmer, a hetero-oligomeric protein complex of seven subunits ( $\alpha$ - $\zeta$  COPs) [6–8]. COPI bud formation is initiated by membrane recruitment of ARF1, which in its GTP-bound form [9, 10], together with members

of the p24 family [11], provides membrane binding sites for coatmer [12]. Subsequent coat assembly leads to membrane deformation and the morphological appearance of a bud [13]. Recently, it was shown that upon interaction with peptides analogous to the cytoplasmic domain of p23 [14], a member of the p24 family, coatmer undergoes a conformational change, which induces the polymerization of the complex [15]. p23, a type I transmembrane protein, is highly enriched in COPI vesicles and is present in a ratio to coatmer of approximately 4:1 [14]. The cytoplasmic domain of p23 (YLRRFFKAKKLIE) contains a classical dilysine motif (KKXX) for retrieval to the endoplasmic reticulum (ER) [16–19], and binds coatmer with the same efficiency as the KKXX motif [14]. p23 binding, however, depends on its phenylalanine residues as well as its lysine residues. A dimeric form of the above mentioned peptide, disulfide-bridged via additional cysteine residues at the N-terminus, is far more efficient in inducing the conformational change of coatmer [15].

In view of the central role of the cytoplasmic domain of p23 in the formation of COPI-coated vesicles, we determined the three-dimensional structure of peptides analogous to this functional domain. The following peptides, known to bind to and to polymerize coatmer, were investigated:

	1	5	9	13
p23wt-m	Y	LRR	FFKAKKLIE	
p23wt-d	CY	LRR	FFKAKKLIE	
	S			
	S			
	CY	LRR	FFKAKKLIE	

We decided to determine the structure of these peptides in the presence of 2,2,2-trifluoroethanol (TFE)

<sup>1</sup>To whom correspondence should be addressed at current address: Institut für Biotechnologie und Wirkstoff-Forschung (IBWF), Erwin-Schrödinger-Strasse 56, D-67663 Kaiserslautern, Germany. Fax: +49-921-3167215. E-mail: mw@ibwf.uni-kl.de.

TABLE I

<sup>1</sup>H Chemical Shifts and Assignments for p23wt-m and p23wt-d, Respectively, 4.0 mM, at 280 K in 100 mM Potassium Phosphate Buffer, 50 mM NaCl, pH 3.6, 40% d<sub>2</sub>-TFE Relative to DSS as an External Standard, ±0.01 ppm

Res.	HN	C <sub>α</sub> H	C <sub>β</sub> H	C <sub>γ</sub> H	Others
p23wt-m					
Y1		4.23	3.17, 3.08		7.12 (H2/6); 6.84 (H3/5)
L2	8.47	4.33	1.62, 1.57	1.48	0.88, 0.84 (δ)
R3	8.39	4.19	1.82, 1.69	1.60	3.17 (δ); 7.33 (ε); 6.83, 6.58 (ηNH)
R4	8.24	4.15	1.71	1.49	3.10 (δ); 7.28 (ε); 6.86, 6.52 (ηNH)
F5	7.9	4.46	3.03, 2.99		7.22 (H3/5); 7.04 (H2/6)
F6	7.99	4.39	3.12, 3.04		7.32 (H3/5); 7.21 (H2/6)
K7	8.08	4.13	1.85, 1.78	1.46, 1.37	1.67 (δ); 2.96 (ε); 7.68 (εNH)
A8	8.03	4.15	1.41		
K9	7.99	4.11	1.78, 1.72	1.34	1.60 (δ); 2.92 (ε); 7.61 (εNH)
K10	7.96	4.2	1.81	1.41	1.68 (δ); 2.95 (ε); 7.63 (εNH)
L11	8.01	4.31	1.7	1.58	0.88, 0.84 (δ)
I12	7.73	4.2	1.87	1.47, 1.13, 0.89	0.84 (δ)
E13	8.03	4.31	1.99	2.43, 2.16	
p23wt-d					
C0		4.43	3.37, 3.24		
Y1	9.09	4.61	3.08		7.10 (H2/6); 6.79 (H3/5)
L2	8.07	4.18	1.63, 1.56	1.49	0.85, 0.79 (δ)
R3	8.01	4.05	1.77	1.52	3.09, 3.06 (δ); 7.33 (ε); 6.83, 6.58 (ηNH)
R4	8.01	4.06	1.85, 1.70	1.62	3.20 (δ); 7.41 (ε); 6.88, 6.60 (ηNH)
F5	7.92	4.33	3.04, 2.95		7.18 (H3/5); 6.97 (H2/6)
F6	8.11	4.31	3.15, 3.07		7.29 (H3/5); 7.22 (H2/6)
K7	8.11	4.12	1.85, 1.68	1.40	1.52 (δ); 2.95 (ε); 7.69 (εNH)
A8	8.06	4.14	1.43		
K9	7.96	4.06	1.77, 1.68	1.27	1.56 (δ); 2.85 (ε); 7.61 (εNH)
K10	7.92	4.15	1.85	1.41	1.67 (δ); 2.95 (ε); 7.62 (εNH)
L11	7.98	4.30	1.70	1.55	0.85, 0.83 (δ)
I12	7.69	4.20	1.86	1.46, 1.11, 0.89	0.83 (δ)
E13	8.03	4.32	1.99	2.44, 2.16	

[20]. Our studies show that the small cytoplasmic tail domains of p23 adopt a tetrameric state, and offer a model how the amino acid residues essential for binding coatomer are positioned within a tetramer on the membrane surface.

## MATERIALS AND METHODS

**Synthetic peptides.** p23wt-m and p23wt-d were obtained as a commercial product (Deutsches Krebsforschungszentrum, Heidelberg). Dimers were formed by disulfide bridges linking the peptides via N-terminally introduced cysteine residues. For this purpose, newly synthesized monomeric peptides were oxidized in 20% dimethyl sulfoxide in water for 48 h. Subsequently the dimers were isolated by high pressure liquid chromatography.

**Nuclear magnetic resonance spectroscopy of p23wt-m and p23wt-d.** The solution structures of p23wt-m and p23wt-d were obtained from 2D <sup>1</sup>H NMR data (4.0 mM peptide, pH 3.6 in 9:1 H<sub>2</sub>O:D<sub>2</sub>O, 8:2 H<sub>2</sub>O:d<sub>2</sub>-TFE, 7:3 H<sub>2</sub>O:d<sub>2</sub>-TFE, or 6:4 H<sub>2</sub>O:d<sub>2</sub>-TFE, 100 mM potassium phosphate buffer, 50 mM NaCl, 280 K. Complete sequence-specific assignments of backbone and side-chain protons were obtained by total correlation spectroscopy (TOCSY) with 80 ms mixing time [21, 22], correlation spectroscopy (COSY) [23], and NOE spectroscopy (NOESY) (mixing times 150 ms and 300 ms) [24]. All spectra were

acquired on a Bruker DRX600 spectrometer using standard pulse sequences [25]. Saturation of the water signal was accomplished by continuous coherent irradiation prior to the first excitation pulse and during the mixing time of the NOESY experiments. 4096 × 512 data points were collected with a spectral width of 6024 Hz in both dimensions. Base-line correction up to 6th order was applied for all 2D spectra in the F2 as well as the F1 dimension. A sinebell-squared filter with a phase shift of π/2, π/4 or π/8 prior to Fourier transformation was used. Zero-filling resulted in a data size of 4096 × 1024 data points in the frequency domain. In addition to the standard Bruker spectrometer control software, the NDEE 2.0 software package (Software Symbiose, Inc., Bayreuth, Germany) was used for data processing. Chemical shift values are reported relative to 2,2-dimethyl-2-silapentane sulfonate.

For structure calculations, only NOEs visible in the spectra recorded in the presence of 40% TFE with 150 ms mixing time were taken into account. Identical calculations combining information obtained in the presence of 20% TFE resulted in virtually identical structures for p23wt-d. The structure of p23wt-m, however, could not be determined at TFE concentrations lower than 40%.

An estimate of secondary structure elements can be obtained from the proton chemical shifts [26–29]. C<sub>α</sub>H resonances shifted to high field relative to the corresponding random coil values [26] indicate local α-helical structure, whereas downfield shifted resonances are typical for local β-sheet conformation. Elements of regular secondary structure are assumed to be present if a deviation from the random

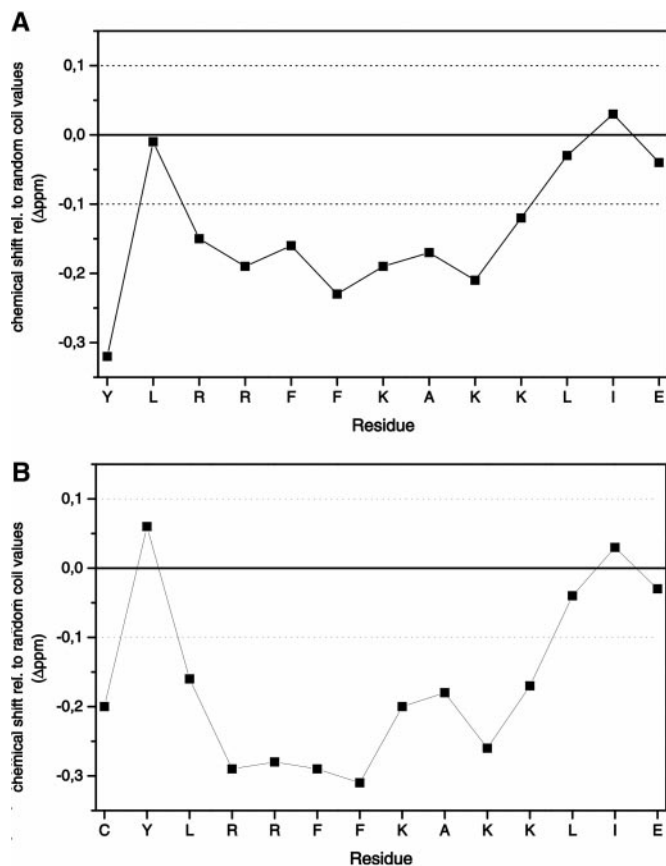


**FIG. 1.** Chemical shift plot of  $C_{\alpha}H(\text{peptide})-C_{\alpha}H(\text{random coil})$  according to [27, 28].

coil value of more than 0.1 ppm is observed. To get a more reliable picture it is suggested [26] that only resonances with the same sense chemical shift deviation for a stretch of more than 3 sequential residues be taken into account.

**Restrained and unrestrained molecular dynamics calculations.** Simulated annealing calculations [30] were performed on SUN workstations with X-PLOR V3.840 [31]. The  $^3J_{\alpha N}$  coupling constants were obtained from cross-peaks in a COSY spectrum. The NOE intensities were classified as strong, medium, and weak and assumed to correspond to proton-proton distances of 1.8–2.7, 1.8–4.0, and 1.8–5.5 Å, respectively. Stereospecific assignments for the methyl, methylene, and aromatic protons have not been performed, and appropriate corrections were added for constraints including pseudoatoms [32–34]. Torsion angles were derived from  $^3J_{\alpha N}$  coupling constants [35]. An interval of  $\pm 30^\circ$  around the experimental value was allowed. Frequency degenerated cross-peaks were incorporated into the structure calculations as ‘ambiguous’ in order to extract as much structural information as possible from the NOESY spectra [31]. Subsequently, the proton-proton distances in the calculated structures were determined using the program “BackCalc\_db 2.0” (Software Symbiose, Inc., Bayreuth, Germany) and compared with the combinations of distances possible for each frequency degenerated NOESY cross-peak. If only one of the possible distance combinations was fulfilled in more than 50% of the calculated structures, the distance information was used in further structure calculations. This procedure was repeated several times.

Elements of regular secondary structure were deduced by chemical shift analysis and the inspection of the NOE pattern. In addition, the structures were checked for the existence of secondary structural



**FIG. 2.** Sequential and medium range NOESY connectivities versus peptide sequence. The height of the bars corresponds to the relative intensity of the NOESY cross-peaks; a gray line indicates that the NOE could not be identified because of spectral overlap. (A) p23wt-m, (B) p23wt-d.

elements by MOLMOL 2.6 [36]. For the unrestrained molecular dynamics simulation (MD) a water/TFE box consisting of 3392 water and 768 TFE molecules with a spatial extension of  $6.2 \times 6.2 \times 6.2$  nm was generated [37, 38]. The structure with the lowest energy was

**TABLE II**  
Energy Contributions to the Structure and Deviations from Standard Geometry

	NOE and X-PLOR statistics	
	p23wt-m	p23wt-d dimer
No. of NOEs		
Total	359	472
$ i - j  = 0$	180	223
$ i - j  = 1$	66	89
$ i - j  = 2, 3, 4, 5$	113	145
$ i - j  > 5$	0	15
Coupling constants	10	0
X-PLOR parameters after SA refinement		
RMSD from ideality		
NOEs (Å)	0.062	0.047
Angles (deg)	0.675	0.655
Bonds (Å)	0.006	0.006
Impr (deg)	0.448	0.442
Dihedral (deg)	1.225	n.a.
Average energies (kJ/mol)		
$E_{\text{total}}$	457	1667
$E_{\text{bonds}}$	45	154
$E_{\text{angles}}$	138	541
$E_{\text{NOE}}$	292	854
RMSD among the 30 structures (nm)		
Backbone	0.0014	0.031
All heavy atoms	0.0084	0.037
NOE violations ( $\geq 0.5$ Å)	0	<2 ( $\approx 0.6$ )
Violations of dihedral angles ( $\geq 30^\circ$ )	0	n.a.

*Note.* All calculations were carried out using the standard X-PLOR force field and energy terms. An SA protocol with subsequent refinement was used to generate 100 structures from an elongated starting conformation. The values are mean values over 30 structures.

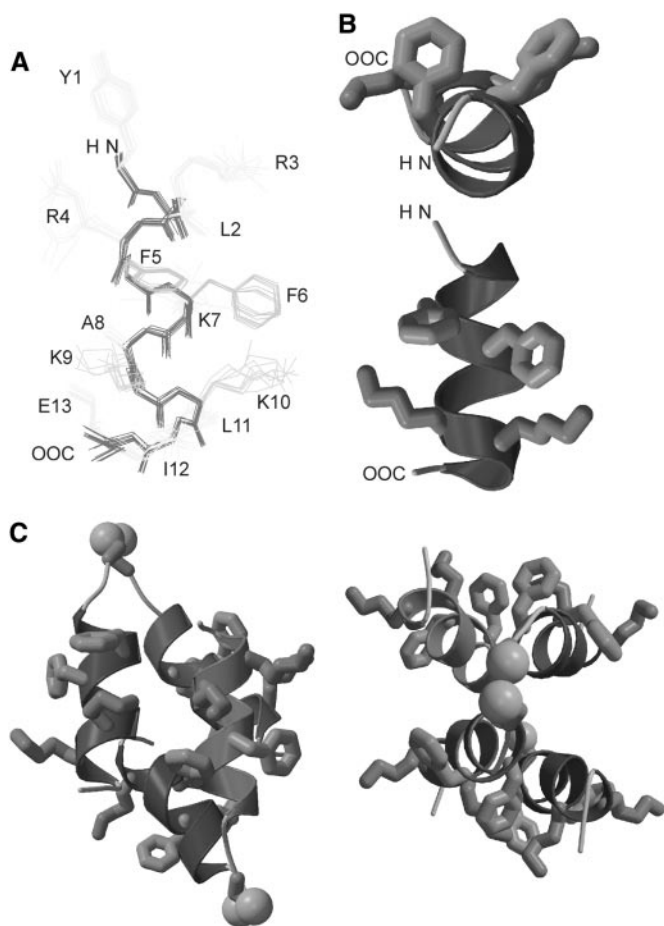


**FIG. 3.** (A) Superimposition of the 10 structures with lowest internal energies of p23wt-m obtained from simulated-annealing molecular dynamics using NOE-derived and dihedral restraints. The heavy atoms of all structures are shown. (B) Ribbons depiction of p23wt-m showing the secondary structure, diphenylalanine and the dilysine motif. Top: view perpendicular to the helix axis; bottom: parallel view. A similar representation from the structure of p23wt-d dimer, representing the tetramer of the cytoplasmic domain of p23, is shown in C.

chosen as the starting structure for the MD calculations. The further calculation strategy was described earlier [37–41].

## RESULTS

Sequence-specific assignments of the spin systems identified in the COSY and TOCSY spectra could be performed with standard techniques [25] as the spectra were well resolved (Table I). Chemical shift data of the  $C_\alpha H$  resonances was analyzed according to the chemical shift index strategy [27,28], yielding an estimate of elements of regular secondary structure (Fig. 1). An  $\alpha$ -helical stretch from R3 to K10 (p23wt-m) and from L2 to K10 (p23wt-d) is clearly suggested. This preliminary estimate was confirmed and refined by analysis of NOESY cross-peak patterns: According to sequential short-range  $d_{NN}(i, i + 1)$  NOEs, medium-

range  $d_{\alpha\beta}(i, i + 3)$ ,  $d_{\alpha N}(i, i + 3)$ , and  $d_{\alpha N}(i, i + 4)$  NOEs (Fig. 2), p23wt-m as well as p23wt-d form  $\alpha$ -helices from L2 to I12, fraying at Y1 and E13.

The solution structure as determined by restrained molecular dynamics calculations (Tables I and II) shows that the four residues involved in coatomer binding, F5, F6, and K9, K10 [14], are located at the same side of a helix (Fig. 3B) that clearly shows amphipathic character, its hydrophobic face composed of residues Y1, F5, A8, and I12. Amphipathicity is increased by a salt bridge between K9 and E13, stable in molecular dynamics simulations (data not shown). The root-mean-square deviation (rmsd) for the backbone heavy atoms of the 30 structures with lowest internal energies of p23wt-m is 0.0014 nm.

The structure of p23wt-d, calculated under the assumption of a monomeric state of the dimerized peptide (data not shown), could not satisfactorily explain 15 long-range NOEs between I12 and Y1, and I12 and F5 (at lower TFE concentrations, 20 and 15% (v/v), additional NOEs between F6 and E13 could be observed). This implies oligomerization of p23wt-d at least to a p23wt-d dimer, analogous to a tetrameric form of the p23 cytoplasmic domain. To analyze this dimerization of p23wt-d biochemically, size exclusion chromatography was performed at pH 7.4 without the addition of TFE and under the conditions used for NMR spectroscopy. Size exclusion chromatography clearly confirms a dimeric state of p23wt-d even in the absence of TFE (Experiments carried out under the conditions used for NMR spectroscopy yielded identical results) [15].

These results clearly show that p23wt-d, the dimerized peptide, is dimerized in solution, i.e., forms a complex of four p23-tail domains. Comparing the experimental NMR spectra with the spectra expected for the four possible structures of a dimer (Fig. 5), only one structure is plausible (Fig. 5D): Structure A cannot

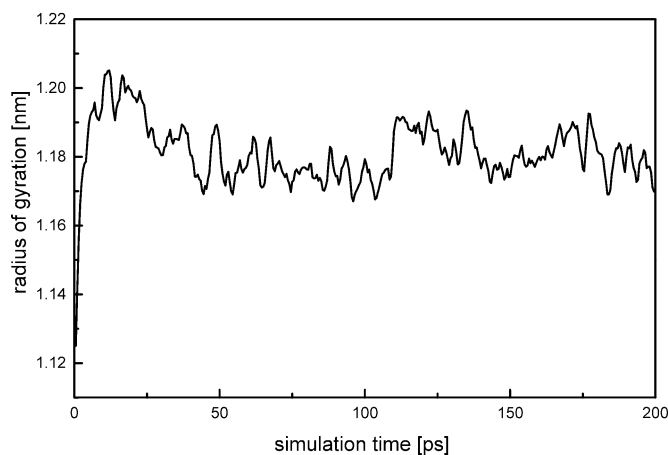


**FIG. 4.** Radius of gyration of p23wt-d during the 200-ps unrestrained molecular dynamics calculation.

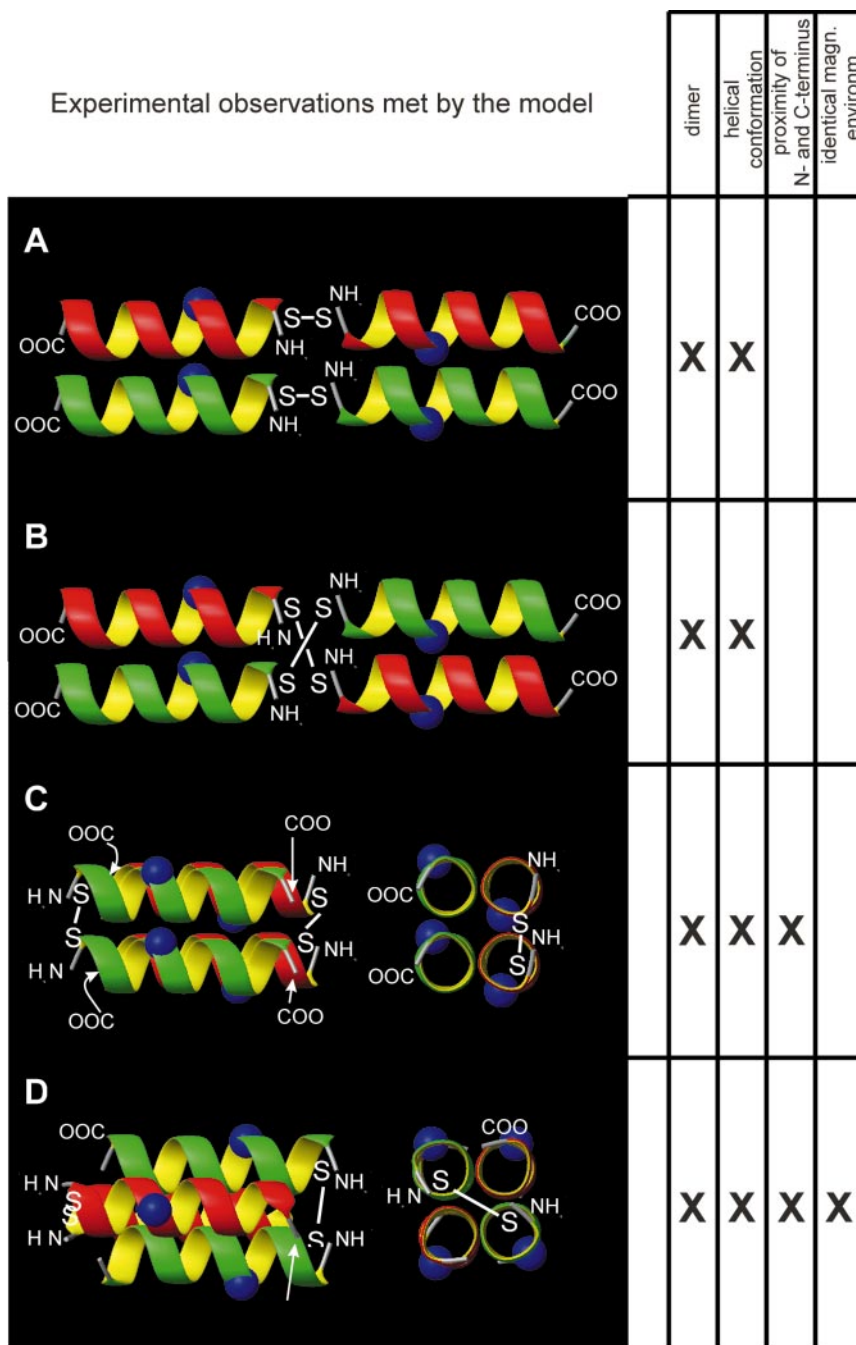


**FIG. 5.** Possible structures of a p23wt-d dimer. The chains of the p23wt-d monomers are shown in green and red, respectively. The blue spheres represent the C $\alpha$ -atoms of K9. Only Model D fulfills all experimental data. MolMol 2.5.1 [36] was used for the generation of the models.

explain the 15 observed NOEs between I12 (close to the COOH-terminus) and Y1 or F5 (close to the NH<sub>2</sub>-terminus). The same is true for Model B. While Model C fulfills the above-mentioned distance restraints, it does not reflect the symmetry detected by NMR spectroscopy. In the NMR spectra the four amino acids with the same sequence position give rise to only one spin system, i.e., the magnetic environment of the four res-

idues must be identical (Fig. 5). Only an arrangement of the two p23wt-d similar to the one depicted in Fig. 5D meets all experimental constraints: (i) dimeric; (ii) helical conformation; (iii) proximity of NH<sub>2</sub>- and COOH-terminus; (iv) an identical magnetic environment for the four helices of a p23wt-d dimer.

In the Clean-TOCSY spectrum of p23wt-d dimer (Fig. 6) three different spin systems, corresponding to

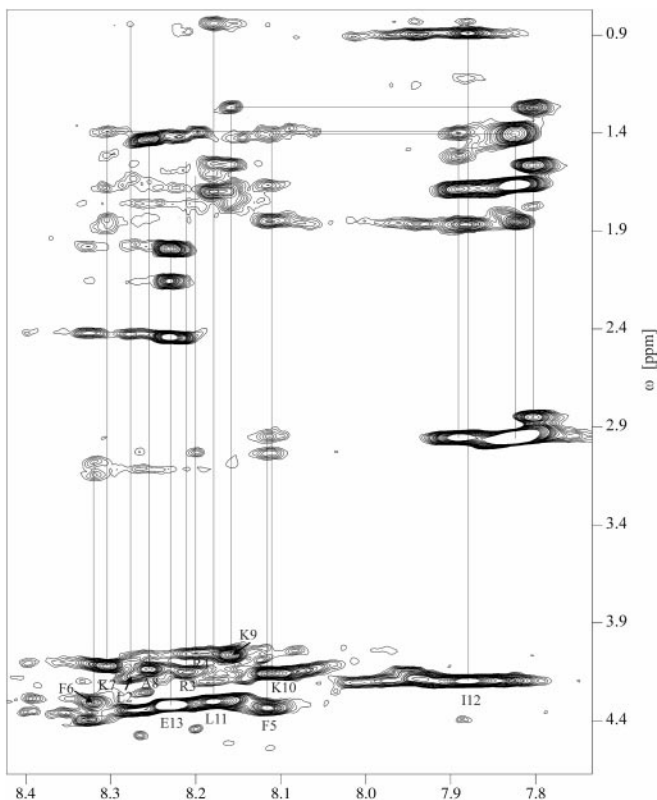


**FIG. 6.** Clean-TOCSY spectrum of p23wt-d. The region of the resonances between amid protons and  $\epsilon$ -NH protons of lysine, respectively, and the protons of the side-chains is shown. Experimental conditions: 4.0 mM p23wt-d; pH 3.6; 6:4 H<sub>2</sub>O:d<sub>2</sub>-TFE; 100 mM potassium phosphate buffer, 50 mM NaCl, 280 K, 80 ms mixing time.

three different conformations, for each of the COOH-terminal residues I12 and E13 are discernible. In both cases, however, only one of the spin systems shows interresidual NOEs, which were used in the structure determination.

The overall structure of the p23wt-d dimer is bipartite (Fig. 3C). The  $\alpha$ -helices are well defined, and a hydrophobic core is created through interactions of the side chains of residues F5, A8, L11, and I12 of the two dimers. A semicircle is formed by residues K9 and K10 of two antiparallel helices (Fig. 3C). The corresponding diphenylalanine motifs of the two antiparallel  $\alpha$ -helices are separated by this "K-semicircle" (Fig. 3C). Thus, p23wt-d dimer comprises a tetramer of the cytoplasmic domain of p23. This is in agreement with the stoichiometry found for both p23 protein and coatomer in isolated COPI vesicles and in coatomer precipitated by p23wt-d [15]. We propose that this tetramer is the species active in coatomer binding *in vivo* (Fig. 7).

The stability of the calculated structure was probed by MD simulations over 200 ps, and in Fig. 4B the radius of gyration, a measure for the compactness of a molecule, as a function of the simulation time is shown. After a rapid increase, which is caused by the equili-

bration of the system, the radius of gyration decreases slightly from 1.20 to 1.18 nm.

## DISCUSSION

The differences between the NOESY pattern of p23wt-m and p23wt-d can easily be explained by slightly different secondary structures and structural stabilities of the two peptides, and by the evaluation strategy of NOESY spectra used in this work. Only NOESY cross-peaks that could unambiguously be assigned to a single proton-proton distance were used for the structure calculations. This strategy prevents the overinterpretation of NOESY spectra, but minor differences in the spectra can result in seemingly very different patterns of sequential and medium range NOESY connectivities (Fig. 2). Despite the dissimilarity of the NOESY pattern of the two peptides, the principal statement is identical: Both peptides adopt an  $\alpha$ -helical conformation. In the TOCSY spectrum of p23wt-d three distinct spin systems, equivalent to distinct conformations of I12 and E13, are discernible, suggesting a higher structural flexibility of these residues. The chemical shift plot (Fig. 1) and the observation that only the spin systems of I12 and E13 labeled in Fig. 6 show interresidual NOESY cross-peaks confirm this notion.

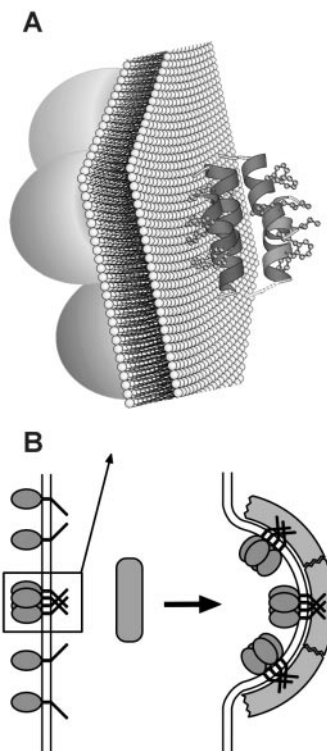


**FIG. 7.** Hypothetical model for bud formation. According to this model, interaction of coatomer with a tetramer of p23 induces a conformational change of the complex. This leads to its polymerization on the surface of a membrane resulting in the formation.

It is also remarkable that the rmsd value of the backbone atoms of p23wt-d dimer is nearly 20 times larger than the value of p23wt-m. The reason for this is easily found in the limited number of inter-monomeric NOESY restraints used in the structure calculation of p23wt-d dimer. This allows slightly different orientations of the helices relative to each other giving rise to the observed rmsd value. The backbone of p23wt-m is well defined by a large number of NOESY cross-peaks and by dihedral restraints which is reflected by its low rmsd value typical for such small peptides (see, e.g., Protein Data Bank entries 1aft, 1aqp, or 3btb).

To avoid misinterpretations based on the influence of TFE on the stability of secondary structure elements [38, 42], we varied the concentration of TFE allowing us to determine the influence of this helix-inducing reagent on the structures of the peptides. At low TFE concentrations, p23wt-m nearly completely lost its regular secondary structure whereas the structures of p23wt-d are virtually identical at 20 and 40%, and even at lower TFE concentration the  $\alpha$ -helical conformation is still present as determined by CD spectroscopy (data not shown). The increased stability of p23wt-d is most probably due to the observed hydrophobic core formed by the dimer. The MD simulations carried out also indicate that the dimer of p23wt-d and hence its hydrophobic core is stable under the conditions chosen for the simulation (Fig. 4B).

The higher efficiency of p23wt-d in precipitating coatomer compared to p23wt-m can easily be explained by the increased structural flexibility of p23wt-m preventing a defined orientation of its binding motifs. Moreover, the structure of p23 that triggers the recently observed conformational change of coatomer [15] is a tetramer of four equivalent  $\alpha$ -helical domains, as judged from nuclear magnetic resonance spectroscopy and molecular dynamics simulations. A tetrameric form of this domain is confirmed by size exclusion chromatography and determination of its stoichiometry in the precipitated coatomer complex [15]. The structure arising from tetramerization of the p23-tail domain represents a symmetrical molecule of two equivalent halves (Fig. 5C). One such motif may be directed toward the surface of the Golgi membrane and may well be stabilized by interactions with membrane lipid head groups, and the other motif may protrude from the membrane and serve as a "plug" for coatomer.

Recently, it was shown that certain aminoglycoside antibiotics and 1,3 cyclohexanebis(methylamine) can bind to coatomer complexes by interacting with their di-lysine binding sites [43, 44]. Furthermore, it was proposed that the distance between two dilysine binding sites was approx. 12 Å. This notion is supported by our study: The distance between the two dilysine motifs in p23wt-d varies from 10 to 15 Å in good agreement with the proposed 12 Å considering the flexibility of a lysine side chain. Combining our results with the

results of [15] leads to the model depicted in Fig. 7. The axes of the four helices should be parallel to the plane of the membrane, otherwise the tetramerization of the p23-tail domain would not be possible. This is due to the restraints that arise from the fact that p23 is a type I transmembrane protein and the antiparallel orientation of the p23wt-d molecules in the structure determined in this study.

## ACKNOWLEDGMENTS

We thank Dr. Heinrich Sticht for his help with the X-PLOR protocols. This work was supported by grants from the Human Frontier Science Program (to F.W.) and the Fonds der Chemischen Industrie (to F.W., P.R.).

## REFERENCES

- Rothman, J. E. (1994) Mechanisms of intracellular protein transport. *Nature* **372**, 55–63.
- Rothman, J. E., and Wieland, F. T. (1996) Protein sorting by transport vesicles. *Science* **272**, 227–234.
- Schekman, R., and Orci, L. (1996) Coat proteins and vesicle budding. *Science* **271**, 1526–1533.
- Serafini, T., Orci, L., Amherdt, M., Brunner, M., Kahn, R. A., and Rothman, J. E. (1991) ADP-ribosylation factor is a subunit of the coat of Golgi-derived COP-coated vesicles: a novel role for a GTP-binding protein. *Cell* **67**, 239–253.
- Taylor, T. C., Kahn, R. A., and Melancon, P. (1992) Two distinct members of the ADP-ribosylation factor family of GTP-binding proteins regulate cell-free intra-Golgi transport. *Cell* **70**, 69–79.
- Waters, M. G., Serafini, T., and Rothman, J. E. (1991). 'Coatomer': a cytosolic protein complex containing subunits of non-clathrin-coated Golgi transport vesicles. *Nature* **349**, 248–251.
- Stenbeck, G., Harter, C., Brecht, A., Herrmann, D., Lottspeich, F., Orci, L., and Wieland, F. T. (1993) beta'-COP, a novel subunit of coatomer. *EMBO J.* **12**, 2841–2845.
- Harter, C. (1995) COP-coated vesicles in intracellular protein transport. *FEBS Lett.* **369**, 89–92.
- Donaldson, J. G., Cassel, D., Kahn, R. A., and Klausner, R. D. (1992) ADP-ribosylation factor, a small GTP-binding protein, is required for binding of the coatomer protein beta-COP to Golgi membranes. *Proc. Natl. Acad. Sci. USA* **89**, 6408–6412.
- Palmer, D. J., Helms, J. B., Beckers, C. J., Orci, L., and Rothman, J. E. (1993) Binding of coatomer to Golgi membranes requires ADP-ribosylation factor. *J. Biol. Chem.* **268**, 12083–12089.
- Stamnes, M. A., Craighead, M. W., Hoe, M. H., Lampen, N., Geromanos, S., Tempst, P., and Rothman, J. E. (1995) An integral membrane component of coatomer-coated transport vesicles defines a family of proteins involved in budding. *Natl. Acad. Sci. USA* **92**, 8011–8015.
- Nickel, W., and Wieland, F. T. (1997) Biogenesis of COPI-coated transport vesicles. *FEBS Lett.* **413**, 395–400.
- Orci, L., Palmer, D. J., Ravazzola, M., Perrelet, A., Amherdt, M., and Rothman, J. E. (1993) Budding from Golgi membranes requires the coatomer complex of non-clathrin coat proteins. *Nature* **362**, 648–652.
- Sohn, K., et al. (1996). A major membrane protein of Golgi-derived COPI-coated vesicles involved in coatomer binding. *J. Cell Biol.* **135**, 1239–1248.
- Reinhard, C., Harter, C., Bremser, M., Brugger, B., Sohn, K.,

- Helms, J. B., and Wieland, F. (1999) Receptor-induced polymerization of coatomer. *Proc. Natl. Acad. Sci. USA* **96**, 1224–1228.
16. Nilsson, T., Jackson, M., and Peterson, P. A. (1989) Short cytoplasmic sequences serve as retention signals for transmembrane proteins in the endoplasmic reticulum. *Cell* **58**, 707–718.
  17. Jackson, M. R., Nilsson, T., and Peterson, P. A. (1993) Retrieval of transmembrane proteins to the endoplasmic reticulum. *J. Cell Biol.* **121**, 317–333.
  18. Jackson, M. R., Nilsson, T., and Peterson, P. A. (1990) Identification of a consensus motif for retention of transmembrane proteins in the endoplasmic reticulum. *EMBO J.* **9**, 3153–3162.
  19. Cosson, P., and Letourneur, F. (1994) Coatomer interaction with di-lysine endoplasmic reticulum retention motifs. *Science* **263**, 1629–1631.
  20. Luo, P., and Baldwin, R. L. (1997) Mechanism of helix induction by trifluoroethanol: A framework for extrapolating the helix-forming properties of peptides from trifluoroethanol/water mixtures back to water. *Biochemistry* **36**, 8413–8421.
  21. Braunschweiler, L., and Ernst, R. R. (1983) Coherence transfer by isotropic mixing: Application to proton correlation spectroscopy. *J. Magn. Reson.* **53**, 521–528.
  22. Griesinger, C., Otting, G., Wüthrich, K., and Ernst, R. R. (1988) Clean TOCSY for  $^1\text{H}$  spin system identification in macromolecules. *J. Am. Chem. Soc.* **110**, 7870–7872.
  23. Jeener, J., Meier, B. H., Bachmann, P., and Ernst, R. R. (1979) *J. Chem. Phys.* **71**, 4546–4553.
  24. States, D. J., Haberkorn, R. A., and Ruben, D. J. (1982) A two dimensional nuclear Overhauser experiment with pure absorption phase in four quadrants. *J. Magn. Reson.* **48**, 286–292.
  25. Wüthrich, K. (1986) *NMR of Proteins and Nucleic Acids*, John Wiley & Sons, New York.
  26. Wishart, D. S., Bigam, C. G., Yao, J., Abildgaard, F., Dyson, H. J., Oldfield, E., Markley, J. L., and Sykes, B. D. (1995)  $^1\text{H}$ ,  $^{13}\text{C}$  and  $^{15}\text{N}$  chemical shift referencing in biomolecular NMR. *J. Biomol. NMR* **6**, 135–140.
  27. Wishart, D. S., Bigam, C. G., Holm, A., Hodges, R. S., and Sykes, B. D. (1995)  $^1\text{H}$ ,  $^{13}\text{C}$  and  $^{15}\text{N}$  random coil NMR chemical shifts of the common amino acids. I. Investigations of nearest-neighbor effects. *J. Biomol. NMR* **5**, 67–81.
  28. Wishart, D. S., Sykes, B. D., and Richards, F. M. (1992) The chemical shift index: A fast and simple method for the assignment of protein secondary structure through NMR spectroscopy. *Biochemistry* **31**, 1647–1651.
  29. Wishart, D. S., Sykes, B. D., and Richards, F. M. (1991) Relationship between nuclear magnetic resonance chemical shift and protein secondary structure. *J. Mol. Biol.* **222**, 311–333.
  30. Nilges, M., Gronenborn, A. M., and Brünger, A. T. (1988) Determination of the three-dimensional structure of proteins from interproton distance restraints. Application to crambin, potato carboxypeptidase inhibitor and barley serine protease inhibitor 2. *Protein Eng.* **2**, 27–38.
  31. Brünger, A. (1993) *X-PLOR 3.1 Manual*, Yale University Press, New Haven, CT.
  32. Clore, G. M., Gronenborn, A. M., Nilges, M., and Ryan, C. A. (1987) Three-dimensional structure of potato carboxypeptidase inhibitor in solution. A study using nuclear magnetic resonance, distance geometry, and restrained molecular dynamics. *Biochemistry* **26**, 8012–8023.
  33. Wagner, G., Braun, W., Havel, T. F., Schaumann, T., Go, N., and Wüthrich, K. (1987) Protein structures in solution by nuclear magnetic resonance and distance geometry. The polypeptide fold of the basic pancreatic trypsin inhibitor determined using two different algorithms, DISGEO and DISMAN. *J. Mol. Biol.* **196**, 611–639.
  34. Qi, P. X., Di Stefano, D. L., and Wand, A. J. (1994) Solution structure of the horse heart ferrocycytochrome c determined by high-resolution NMR and restrained simulated annealing. *Biochemistry* **33**, 6408–6417.
  35. Pardi, A., Billeter, M., and Wüthrich, K. (1984) Calibration of the angular dependence of the amide proton-Ca proton coupling constants,  $^3J_{\text{HN}\alpha}$ , in a globular protein. *J. Mol. Biol.* **180**, 741–751.
  36. Koradi, R., Billeter, M., and Wüthrich, K. (1996) MOLMOL: A program for display and analysis of macromolecular structures. *J. Mol. Graph.* **14**, 51–55.
  37. Jorgensen, W. L., Chandrasekhar, J., Madura, J., Impey, R. W., and Klein, M. L. (1983) Comparison of simple potential functions for simulating liquid water. *J. Chem. Phys.* **79**, 926–935.
  38. Sticht, H., Willbold, D., and Rosch, P. (1994) Molecular dynamics simulation of equine infectious anemia virus Tat protein in water and in 40% trifluoroethanol. *J. Biomol. Struct. Dyn.* **12**, 19–36.
  39. Powell, M. J. D. (1977) Restart procedures for the conjugate gradient method. *Math. Progr.* **12**, 241–254.
  40. Verlet, L. (1967) Computer “experiments” on classical fluids. I. Thermodynamical properties of Lennard-Jones molecules. *Phys. Rev.* **159**, 98–103.
  41. van Gunsteren, W. F., and Berendsen, H. J. C. (1977) Algorithms for macromolecular dynamics and constraint dynamics. *J. Mol. Phys.* **34**, 1311–1327.
  42. Weidler, M., Marx, U. C., Seidel, G., Schafer, W., Hoffmann, E., Esswein, A., and Rosch, P. (1999) The structure of human parathyroid hormone-related protein(1-34) in near-physiological solution. *FEBS Lett.* **444**, 239–244.
  43. Hu, T., Kao, C. Y., Hudson, R. T., Chen, A., and Draper, R. K. (1999) Inhibition of secretion by 1,3-Cyclohexanebis(methylamine), a dibasic compound that interferes with coatomer function. *Mol. Biol. Cell* **10**, 921–933.
  44. Hudson, R. T., and Draper, R. K. (1997) Interaction of coatomer with aminoglycoside antibiotics: Evidence that coatomer has at least two dilysine binding sites. *Mol. Biol. Cell* **8**, 1901–1910.